Atmos. Chem. Phys., 13, 7097–7114, 2013
www.atmos-chem-phys.net/13/7097/2013/
doi:10.5194/acp-13-7097-2013

Atmospheric Chemistry and Physics Open Access

Dust vertical profile impact on global radiative forcing estimation using a coupled chemical-transport–radiative-transfer model

L. Zhang[1,2,3], **Q. B. Li**[1,2], **Y. Gu**[1,2], **K. N. Liou**[1,2], **and B. Meland**[3]

[1]Department of Atmospheric and Oceanic Sciences, University of California, Los Angeles, CA 90095, USA
[2]Joint Institute for Regional Earth System Science and Engineering, University of California, Los Angeles, CA 90095, USA
[3]Department of Mechanical Engineering, University of Colorado, Boulder, CO 80309, USA

Correspondence to: L. Zhang (li.zhang@colorado.edu)

Received: 28 November 2012 – Published in Atmos. Chem. Phys. Discuss.: 23 January 2013
Revised: 20 June 2013 – Accepted: 21 June 2013 – Published: 29 July 2013

Abstract. Atmospheric mineral dust particles exert significant direct radiative forcings and are important drivers of climate and climate change. We used the GEOS-Chem global three-dimensional chemical transport model (CTM) coupled with the Fu-Liou-Gu (FLG) radiative transfer model (RTM) to investigate the dust radiative forcing and heating rate based on different vertical profiles for April 2006. We attempt to actually quantify the sensitivities of radiative forcing to dust vertical profiles, especially the discrepancies between using realistic and climatological vertical profiles. In these calculations, dust emissions were constrained by observations of aerosol optical depth (AOD). The coupled calculations utilizing a more realistic dust vertical profile simulated by GEOS-Chem minimize the physical inconsistencies between 3-D CTM aerosol fields and the RTM. The use of GEOS-Chem simulated vertical profile of dust extinction, as opposed to the FLG prescribed vertical profile, leads to greater and more spatially heterogeneous changes in the estimated radiative forcing and heating rate produced by dust. Both changes can be attributed to a different vertical structure between dust and non-dust source regions. Values of the dust vertically resolved AOD per grid level (VRAOD) are much larger in the middle troposphere, though smaller at the surface when the GEOS-Chem simulated vertical profile is used, which leads to a much stronger heating rate in the middle troposphere. Compared to the FLG vertical profile, the use of GEOS-Chem vertical profile reduces the solar radiative forcing at the top of atmosphere (TOA) by approximately 0.2–0.25 $\mathrm{W\,m^{-2}}$ over the African and Asian dust source regions. While the Infrared (IR) radiative forcing decreases 0.2 $\mathrm{W\,m^{-2}}$ over African dust belt, it increases 0.06 $\mathrm{W\,m^{-2}}$ over the Asian dust belt when the GEOS-Chem vertical profile is used. Differences in the solar radiative forcing at the surface between the use of the GEOS-Chem and FLG vertical profiles are most significant over the Gobi desert with a value of about 1.1 $\mathrm{W\,m^{-2}}$. The radiative forcing effect of dust particles is more pronounced at the surface over the Sahara and Gobi deserts by using FLG vertical profile, while it is less significant over the downwind area of Eastern Asia.

1 Introduction

Mineral dust produced by the wind erosion of dry soil particles at the land surface has been recognized as a leading contributor to global total aerosol loading (Andreas, 1995; Tegen et al., 1997; Miller et al., 2006). Quantifying the impact of mineral dust on radiative forcing is important for understanding past climate and is necessary for the projection of future climate changes (IPCC, 2007). Model studies have suggested that the direct radiative forcing of dust on regional and global scales may be comparable to, or even exceed, the forcing by anthropogenic aerosols (Tegen and Fund, 1995; Li et al., 1996; Sokolik and Toon, 1996; Tegen et al., 1996). Using a radiative transfer model embedded in a general circulation model, Tegen et al. (1996) found that the dust particles from disturbed soils cause a decrease in net global average radiative forcing of about 1 $\mathrm{W\,m^{-2}}$ at the surface.

The optical and physical properties (shape, size distribution and refractive index) of dust particles as well as their vertical distribution constitute the basic parameters in determining radiative forcing and the subsequent feedback to dynamic

and climate systems. The vertical distribution of aerosols is especially important as it modifies the vertical profile of radiative heating in the atmosphere (e.g., Léon et al., 2002; Won et al., 2004; Ramanathan et al., 2007; Johnson et al., 2008), thereby changing atmospheric stability and convection (McFarquhar and Wang, 2006). In addition, it influences the radiative effect at the top of the atmosphere (TOA), particularly when the aerosols have strong absorption of solar radiation (Meloni et al., 2005; Gadhavi and Jayaraman, 2006; Johnson et al., 2008). The dust particles also play important roles in serving as cloud condensation nuclei (Li et al., 2011), thus their vertical distributions relative to cloud cover could impact radiative transfer.

In the evaluation of the radiative impact of dust particles, a primary concern is the uncertainty in the observed vertical structure of the dust distributions (Hamonou et al., 1999). A number of field programs have been carried out to measure the vertical distribution of aerosols, including the Dust and Biomass-burning Experiment (DABEX), Tropospheric Aerosol Radiative Forcing Observation Experiment (TARFOX), and Puerto Rico Dust Experiment (PRIDE) (Hueber et al., 1998; Russell et al., 1999; Maring et al., 2003; Johnson et al., 2008). These ground-based and/or aircraft measurements have provided valuable information, but are limited in spatial and temporal coverage. The space borne lidar systems, such as the Geoscience Laser Altimeter System (GLAS) and the Cloud-Aerosol Lidar and Infrared Pathfinder Satellite Observation (CALIPSO), have provided measurements of the aerosol vertical profiles; however, data coverage is limited due to their narrow footprint and on track pattern (Chaudhry et al., 2007). Although conventional satellite radiometers (e.g., MODIS) have provided aerosol data over the globe scale, only column integrated dust properties have been retrieved in terms of optical thickness (Chu et al., 2002; Kahn et al., 2005). The production of the dust AOD requires a large array of assumptions and approximations (Wielicki et al., 1996). By integrating the available dust information from the preceding observations and constraints into an evolving three-dimensional picture, aerosol transport models can provide a complementary approach to evaluate aerosol radiative forcing (Meloni et al., 2005; Miller et al., 2006).

Some of the general circulation models and RTMs simply assume a prescribed vertical weighting profile of extinction based on "climatology" that does not vary in space and time (Haywood et al., 1999; Gu et al., 2006; McComiskey et al., 2008). However, dust vertical distributions can be modified by numerous dynamical processes and can be quite different over dust source regions and downwind areas as documented by a number of previous studies (e.g., Karyampudi et al., 1999; Su and Toon, 2011). Recently, though many current general circulation models with an online calculation of radiative effects for dust and other aerosols have already include horizontal and vertical aerosol distribution computed by the model (Koffi et al., 2012; Myhre et al., 2013), the results are quite sensitive to the performance of dust simulations, especially the vertical distribution of dust. GEOS-Chem is a global 3-D CTM, which has been employed to simulate instantaneous vertical profiles of dust extinction coefficients with explicit vertical distributions based on aerosol concentrations and optical properties (Tegen and Lacis, 1996). The dust simulation in GEOS-Chem has been able to capture the magnitude and seasonal cycle of dust over the northeast Pacific and the timing and vertical structure of dust outflow in the free troposphere from Asia (Fairlie et al., 2007). Moreover, the positive biases of the dust simulations of both concentration and AOD in GEOS-Chem over the dust source regions and downwind areas (Generoso et al., 2008; Fairlie et al., 2010; Johnson et al., 2012; Ridley et al., 2012; Wang et al., 2012) have been improved in our current study.

The present study is a sensitivity study to examine the radiative forcing of dust to its vertical profiles over different areas, which seeks to develop a more realistic simulation of dust to quantify the discrepancies and sensitivities of assuming a "climatological" dust vertical profile versus using a more realistic 3-D dust vertical profile simulated by GEOS-Chem. In these simulations, dust emissions have been constrained by observed AOD to improve our understanding and estimation of global dust radiative forcing and heating rates.

In this study, a global 3-D GEOS-Chem CTM with improved dust emission algorithms has been coupled with the Fu-Liou-Gu RTM (Gu et al., 2010, 2011) to examine the instantaneous dust radiative forcing in April 2006. A description of the models and the validation of dust simulation are presented in Sect. 2. Section 3 compares the dust vertically resolved AOD per grid level (VRAOD) by using different vertical profiles. The impacts of different dust vertical profiles on the radiative forcing and heating rate are discussed in Sects. 4 and 5. Summary and discussion are given in Sect. 6.

2 Model description

2.1 GEOS-Chem

GEOS-Chem is a global 3-D CTM driven by assimilated meteorological observations from the Goddard Earth Observing System (GEOS) of the NASA Global Modeling and Assimilation Office (GMAO) (Bey et al., 2001). We use GEOS-Chem version 8-01-04 (http://acmg.seas.harvard.edu/geos/) driven by GEOS-5 meteorological fields with 6 h temporal resolution (3 h for surface variables and mixing depths), 2° (latitude) × 2.5° (longitude) horizontal resolution, and 47 vertical layers between the surface and 0.01 hPa. The GEOS-Chem model includes a fully coupled treatment of tropospheric ozone-NO_x-VOC chemistry and sulfate, nitrate, ammonium, organic carbon, black carbon, mineral dust, and sea salt aerosols (Park et al., 2003, 2004; Alexander et al., 2005; Fairlie et al., 2007). The aerosol optical depth at 550 nm is calculated online assuming log-normal size distributions of externally mixed aerosols and is a function of the local

relative humidity to account for hygroscopic growth (Martin et al., 2003). The wet deposition scheme is described by Liu et al. (2001) in GEOS-Chem for water-soluble aerosols, which includes scavenging in convective updrafts and rainout and washout from large-scale precipitation and convective anvils. Dry deposition is based on the resistance-in-series scheme of Wesely (1990) as implemented by Wang et al. (1998).

Dust in GEOS-Chem is distributed in 4 size bins (radii 0.1–1.0, 1.0–1.8, 1.8–3.0, and 3.0–6.0 µm), following Ginoux et al. (2004). The smallest size bin is further divided equally into four sub-micron size bins (with effective radii centered at 0.15, 0.25, 0.4 and 0.8 µm) for determining optical properties and heterogeneous chemistry (Fairlie et al., 2010; Ridley et al., 2011). We use the dust entrainment and deposition (DEAD) mobilization scheme of Zender et al. (2003), combined with the source function used in Global Ozone Chemistry Aerosol Radiation and Transport (GOCART) model (Ginoux et al., 2001; Chin et al., 2004), as described by Fairlie et al. (2007). The optical properties for mineral dust used for the standard GEOS-Chem simulation are based on the refractive indices of Patterson et al. (1977). There is growing recognition that the imaginary component of the refractive index may be too high at UV wavelengths (Colarco et al., 2002). A Mie algorithm (de Rooij and van der Stap, 1984; Mishchenko et al., 1999) is instead used to calculate the optical properties of mineral dust based on the refractive indices of Sinyuk et al. (2003); the single scattering albedo of mineral dust at 300 nm increases by 0.14 to the range of 0.7–0.9 using these new refractive indices (Lee et al., 2009).

2.2 Constraining dust emission using observed AOD

Large discrepancies exist between simulated and observed dust AOD which are related to the uncertainties of dust emission (Generoso et al., 2008; Johnson et al., 2012; Ridley et al., 2012). A factor of three reduction of dust emission has been recommended for the Saharan dust sources region (Generoso et al., 2008). Here we seek to use observed AOD to constrain dust emissions and the GEOS-5 meteorological fields are selected to drive the GEOS-Chem model since it is expected to yield a more realistic representation of the vertical structure of mineral dust in GEOS-Chem (Johnson et al., 2012). The observation data used to constrain dust emission is based on the satellite measurements of Multi-Angle Imaging SpectroRadiometer (MISR) AOD (Martonchik et al., 2004; Kahn et al., 2005).

$$\text{Emission}_{\text{adjusted}} = \text{Emission}_{\text{original}} \times \frac{\text{MISR}_{\text{monthly AOD}}}{\text{Model}_{\text{monthly AOD}}} \quad (1)$$

We apply monthly MISR-to-model AOD ratios (see Eq. 1) for individual grid boxes only over model dust source regions to constrain the dust emissions in each grid box. Figure 1 shows global dust emission for April 2006 after using

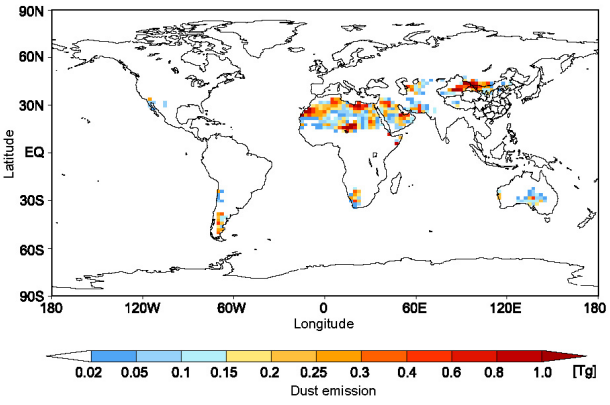

Fig. 1. GEOS-Chem simulated dust emission [Tg] for April 2006.

MISR AOD to constrain the global dust emissions. The simulated global dust emission for April 2006 is 92 Tg, which is reduced more than 40 % compared to 162 Tg before adjustment. Using the adjusted dust emission, it provides better simulations and reduces the particularly pronounced overestimations. The daily surface $PM_{2.5}$ dust concentrations over the western coastal US during spring (March–May) 2006 are in good agreement with the Interagency Monitoring of Protected Visual Environments (IMPROVE) observations (Fig. 2). Figure 3 illustrates the vertically integrated column value of simulated dust AOD for April 2006 before and after emission adjustment and the comparison to MISR AOD. High AOD values are located not only over the dust source regions but also over the surrounding downwind areas, which reflect the impact of transport. The positive bias is particularly pronounced over the Saharan and Gobi dust source regions (see Fig. 3), where model-predicted AOD values are a factor of 2 to 3 higher (Johnson et al., 2012). After adjusting the emission, the significant positive biases of AOD over dust source regions are reduced. Here the MISR AOD includes all aerosols while only dust is considered in the simulated AOD. This would result in the low bias of AOD for the model over ocean and some downwind areas.

The Cloud-Aerosol Lidar and Infrared Pathfinder Satellite Observations (CALIPSO) was launched 2006, which provides measurements of global vertical profiles of aerosol backscatter and extinction in addiction to total column AOD from June 2006 (Young and Vaughan, 2009). The comparisons of dust vertical extinction along 15° N and 40° N between CALIPSO measurements of Level 3 data and the emission-adjusted simulation for July 2006 are shown in Fig. 4. The GEOS-Chem simulation utilizing adjusted emissions is able to reproduce the vertical structure of dust extinction over the African and Asian dust source regions. The maximum centers are quite consistent in the cross sections. Only the simulated dust extinction at low altitudes over the Atlantic is less well represented with negative bias, which is also pointed out by Ridley et al. (2012). Based on the above

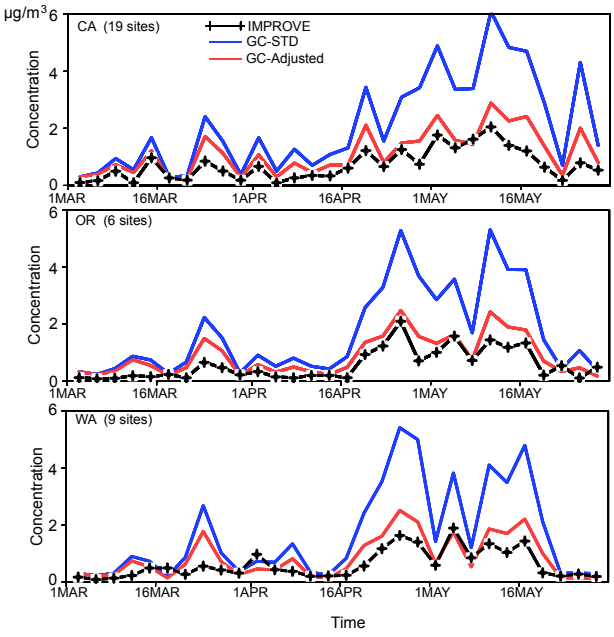

Fig. 2. Simulated and observed (black dot line) surface dust concentration ($\mu g\,m^{-3}$) at representative IMPROVE sites by the states of CA, OR, WA from March to May 2006. The simulated results are based on GEOS-Chem standard simulation GC-STD (blue line) and the emission-adjusted simulation GC-Adjusted (red line).

comparison, it indicates the model is capable of reproducing much of the dust vertical profile and horizontal distribution by using the adjust emission.

2.3 Fu-Liou-Gu radiative transfer model

The atmospheric radiative transfer calculations are performed using the Fu-Liou-Gu (FLG) radiative transfer model (RTM), which is a modified and improved version based on the original Fu-Liou scheme (Fu and Liou, 1992, 1993; Gu et al., 2003, 2006, 2010, 2011). A combination of the delta-four-stream approximation for solar flux calculations (Liou et al., 1988) and delta-two/four-stream approximation for Infrared (IR) flux calculations (Fu et al., 1997) is employed in the model to assure both accuracy and efficiency. The incorporation of non-gray gaseous absorption in multiple-scattering atmospheres is based on the correlated k distribution method developed by Fu and Liou (1992). Parameterization of the single-scattering properties for cloud particles is implemented by following the procedure developed by Fu and Liou (1993). To increase computational accuracy, the similarity principle for radiative transfer is applied to each grid point to account for the fractional energy in the diffraction peak of the phase function. The solar (0–5 μm) and IR (5–50 μm) spectra are divided into 6 and 12 bands, respectively, according to the location of prominent atmospheric absorption bands. In the solar spectrum, absorption due to water vapor, O_3, CO_2, O_2, and other minor gases, such as CO, CH_4, and N_2O, is taken into account. Absorption due to water vapor, O_3, CO_2, CH_4, N_2O and CFCs is also considered in the IR spectrum.

In the radiation scheme, a total of 18 aerosol types have been parameterized by employing the Optical Properties of Aerosols and Clouds (OPAC) database (d'Almeida et al., 1991; Tegen and Lacis, 1996; Hess et al., 1998), which provides the single scattering properties for spherical aerosols computed from the Lorenz–Mie theory in which humidity effects are accounted for. The single scattering properties of the 18 aerosol types for 60 wavelengths in the spectral region between 0.3 μm and 40 μm are interpolated into the 18 Fu-Liou (Fu and Liou, 1992) spectral bands of the current radiation scheme (Gu et al., 2006). Aerosol types include maritime, continental, urban, five different sizes of mineral dust, insoluble, water soluble, soot (BC), sea salt in two modes (accumulation mode and coarse mode), mineral dust in four different modes (nucleation mode, accumulation mode, coarse mode, and transported mode), and sulfate droplets.

In the current FLG-RTM, the input AOD represents the vertically integrated column value, which has been distributed vertically according to a certain weighting profile based on the layer pressure and scale height (height at which the aerosol loading is reduced to e^{-1} of the surface value) (Gu et al., 2006). The aerosol loading decreases exponentially and the highest aerosol layer in the model is placed at 15 km (Charlock et al., 2004). This represents a set of distributions that can be simply described by an exponential function with different scale heights. Such vertical distributions are typically used by radiative transfer models (e.g., McComiskey et al., 2008) and can be traced back to the work of Elterman (1968). In this study, the visible surface albedo and the atmospheric vertical profiles of pressure, temperature, water vapor, and O_3 provided by GEOS-Chem meteorological data and simulation are used to drive the FLG-RTM.

In the current study, the spatial variations of solar zenith angle and emissivity are not taken into account. Here the cosine of the solar zenith angle of 0.5 and emissivity of 1 are used in the calculations. Normally, the global estimate of monthly mean aerosol forcings may not be very accurate by using a constant solar zenith angle throughout the simulation. However, the purpose of this study is to assess the sensitivity of radiative forcing to different vertical profiles of dust extinction. Since the cosine of solar zenith angle only affects the available solar flux at the TOA, the spatial and temporal variations of the solar flux at the TOA due to variations of the solar zenith angle would be the same in the two simulations using different vertical aerosol profiles. The same column-integrated AOD of dust simulated by GEOS-Chem (Fig. 2b) is used as the input to calculate the radiative forcing except for the different vertical profile of dust extinction. One profile is based on the default vertical weighting of dust extinction in FLG as mentioned above. The other is according to the simulated vertical profile of extinction in GEOS-Chem. The

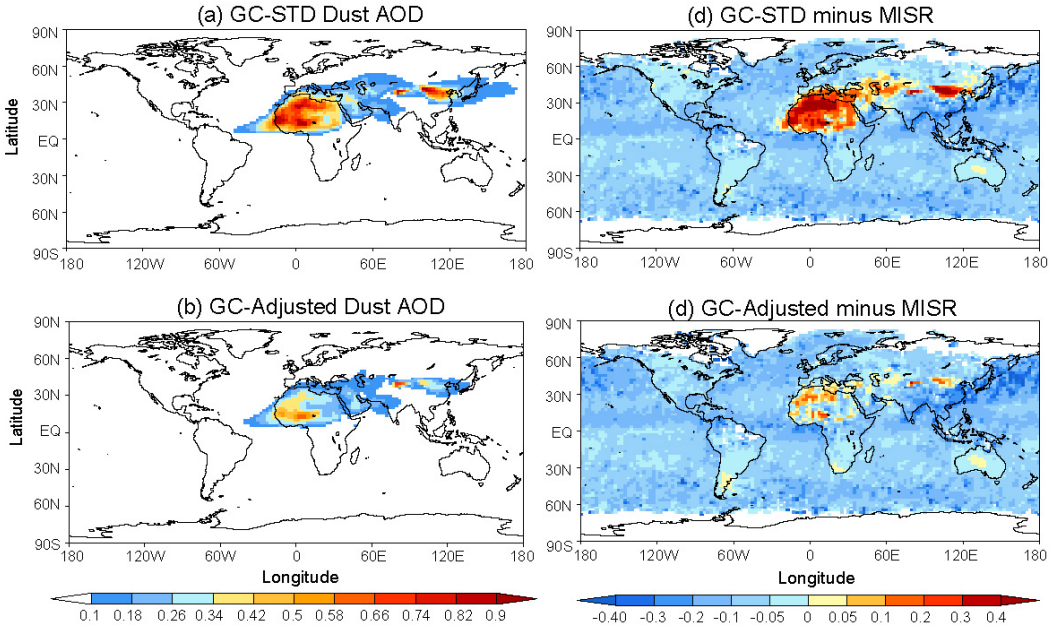

Fig. 3. Comparisons of MISR AOD and GEOS-Chem dust AOD for April 2006. **(a)** GEOS-Chem dust AOD with standard simulation; **(b)** GEOS-Chem dust AOD with adjusted emission; **(c)** GEOS-Chem dust AOD with standard simulation minus MISR AOD and **(d)** GEOS-Chem dust AOD with adjusted emission minus MISR AOD.

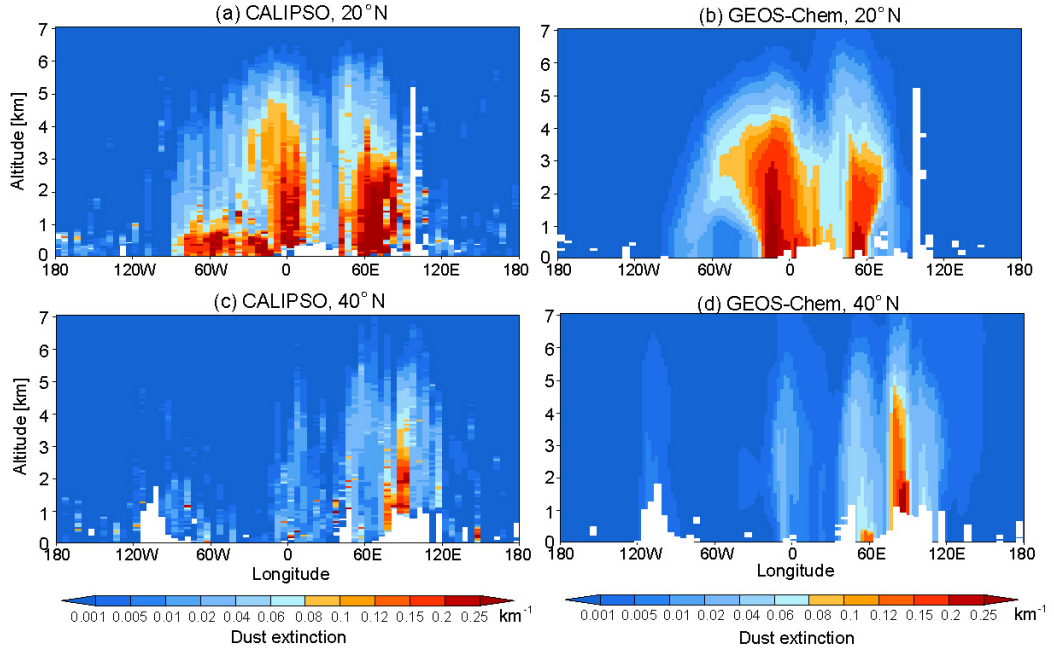

Fig. 4. Cross sections of CALIPSO and GEOS-Chem dust extinction (km^{-1}) for July 2006 along 20° N and 40° N.

present study will focus on the instantaneous monthly mean results of April 2006.

3 Dust sources and VRAOD using different vertical profiles

The deserts of North Africa and Asia represent the major dust sources with North Africa contributing about 1400 Tg yr^{-1}

(65 % of the global emission) while the deserts of Asia (including the Gobi and Takla Makan deserts) contribute around 25 % (Ginoux et al., 2004). Figure 1 illustrates the dust sources over the world, which shows two major dust regions over Africa and Asia. The African and Asian deserts are in different meteorological regimes due to their latitudinal differences. The African dust belt includes the Sahara desert and the arid regions in Arabia. During the cool season from November to April, the synoptic scale cyclones in the northern sector of the Sahara are able to cause widespread dust emission over Libya and Egypt (Bou Karam et al., 2010). Then the intensified Libyan high and African easterly waves induce dust outbreaks and activating dust sources in Mauritania, Mali, and Algeria (Knippertz and Todd, 2010). The Low-level jets (LLJs) and cold pools of mesoscale convective systems also play important roles in affecting diurnal and seasonal characteristics of Saharan dust emission, dust devils and dusty plumes, as well as transport (Koch and Renno, 2005; Washington et al., 2006; Schepanski et al., 2009; Knippertz and Todd, 2012). In addition, the deep convection and strong winds embedded in the trades (northeasterly flow) would result in Saharan dust lifting occurring all year long (Su and Toon, 2011). The Taklimakan and Gobi desert are the major constitutors of the Asian dust belt (Uno et al., 2005). The seasonal variation of dust outbreaks in Asia is associated with the seasonal modulation of the wind speed (Su and Toon, 2011). The soil conditions and mid-latitude cyclones accompanied by strong surface winds are related to the occurrences of dust storms over the Asian source region (Zhao and Zhao, 2006). The following analysis will focus on these two major dust belts, defined as the African dust belt (10–35° N) and the Asian dust belt (35–45° N), respectively, in order to better distinguish their characteristics.

The VRAOD varies dramatically depending on whether the GEOS-Chem simulated or the FLG default vertical profile is used in the radiative transfer calculations. The altitude–longitude cross sections are averaged over the African dust belt and the Asian dust belt (Fig. 5) With the GEOS-Chem vertical profile, a deep mixed layer of the Saharan air layer (SAL) is prominent. SAL is a dry and well-mixed layer that often extends to ∼ 500 hPa over Africa (Carlson and Prospero, 1972), and occurs during late spring through early fall over extensive portions of the north Atlantic Ocean between the Sahara desert, western Indies and the United States (Prospero and Carlson, 1972). The maximum of dust VRAOD are consistent from surface to 600 hPa with the maximum of more than 0.015 (see Fig. 5a) since the Saharan dust source region is primarily located in a deep layer of SAL (Su and Toon, 2011). Moreover, the SAL shows a peculiar vertical profile characterized by a large aerosol concentration in the mid-troposphere, which is significantly different from the non-dust source regions. There are three main transport pathways from the African dust source region: westward across the Atlantic to the Americas, eastward across the eastern Mediterranean to the Middle East and Asia, and northward across the Mediterranean to Europe (McKendry et al., 2007). The westward and eastward pathways are evident in the altitude–longitude cross section of dust VRAOD using GEOS-Chem profile.

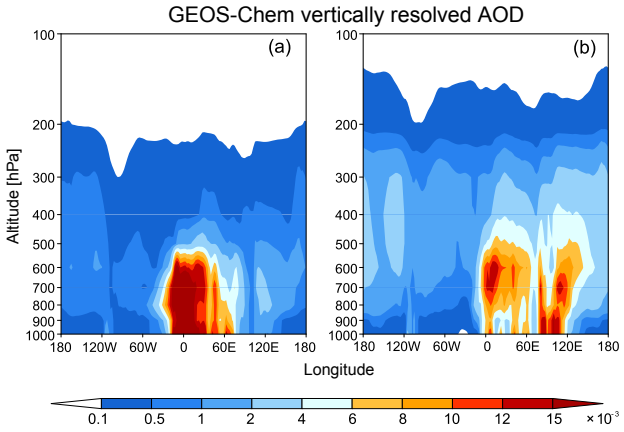

Fig. 5. Altitude–longitude cross sections of dust VRAOD averaged over **(a)** African dust belt (10–35° N) and **(b)** Asian dust belt (35–45° N) by using GEOS-Chem vertical profile.

Dust originating from Asian source regions shows different vertical distributions. The average of VRAOD over the Asian dust belt is shown in Fig. 5b. As presented by previous study (Su and Toon, 2011), two evident dust layers with large values of dust VRAOD are seen at different altitudes. One is located over the Gobi desert (90–110° E), with the high dust VRAOD extending from the surface to 800 hPa. The other is above the boundary layer in the middle troposphere with the maximum at 700 hPa. This dust layer is located in the downwind areas of the source region to the east of the Gobi desert. Horizontal wind shear plays an important role in producing the elevated dust layer over Asia (Su and Toon, 2011). The maximum VRAOD over the Asian source region is much lower than that of the African source region. In addition, there is another widespread high dust VRAOD in the middle troposphere over a broad swath from 5° W to 60° E over the southern Europe. As the non-dust source regions, this maximum VRAOD reflects the impact of transport of eastward and northward pathways from the African source region. The other maximum VRAOD over the non-dust source regions is located over the major transport pathway, which is eastward on the mid-latitude at a considerable distance from the Asian source regions (McKendry et al., 2007).

The altitude–longitude cross sections of dust VRAOD, averaged over African and Asian dust belts using the FLG vertical profile, are shown in Fig. 6. Different from that in the GEOS-Chem vertical profile, the maximum VRAOD is close to the surface and the characteristics of the SAL are not reproduced. The FLG vertical profile decreases with increasing altitude globally, including both the dust and non-dust source regions. The deficiency is evident in using such prescribed

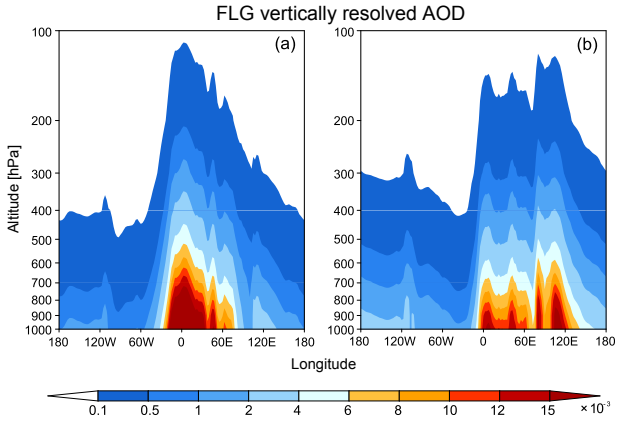

Fig. 6. Altitude–longitude cross sections of dust VRAOD averaged over **(a)** African dust belt (10–35° N) and **(b)** Asian dust belt (35–45° N) by using FLG vertical profile.

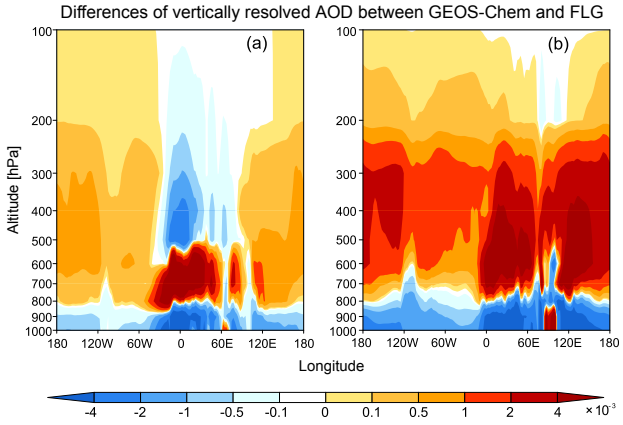

Fig. 7. Differences of dust VRAOD between using GEOS-Chem vertical profile and FLG vertical profile (former minus latter) averaged over **(a)** African dust belt (10–35° N) and **(b)** Asian dust belt (35–45° N).

"climatological" vertical profiles since the non-dust source regions and ocean areas have the same vertical profiles as those of the dust source regions with the maximum VRAOD at the surface. Moreover, none of the transport pathways from source regions have been indicated.

The differences in the dust VRAOD between using GEOS-Chem or FLG vertical profile, assuming the same column-integrated AOD (as shown in Fig. 3b), over the African and Asian dust belts are shown in Fig. 7. Using the GEOS-Chem vertical profile for the African dust belt produces much higher VRAOD in the middle troposphere (800–550 hPa); up to a factor of 2 higher than from using the FLG vertical profile. Much lower dust VRAOD are shown in the low troposphere (1000–800 hPa) and above 550 hPa over the North African areas (20° W–40° E). The positive differences of dust VRAOD are shown in the middle to upper troposphere over areas downwind of the African dust belt. This suggests that more dust particles might be lifted into the free troposphere using the GEOS-Chem vertical profile (Fig. 7a). These differences are more significant over the Asian dust belt (Fig. 7b). The values of dust VRAOD are increased by a factor of 5 in the middle to upper troposphere using GEOS-Chem vertical profile over the Asian dust source region and downwind areas. Similarly, the dust VRAOD averaged over the Asian dust belt is much lower near the surface layer (1000–800 hPa) using the GEOS-Chem vertical profile. Obviously, the impact of dust transport is not reflected by using FLG vertical profile, which results in significant differences compared to the GEOS-Chem vertical profile along downwind areas of source regions.

The simulated dust VRAOD is the sum of VRAOD for each size bin. The smallest (0.7 µm) dust particles play important roles in contributing to the large values of VRAOD over the African and Asian dust source regions primarily due to large particles in the coarse mode being removed by gravitational settling. The differences of dust VRAOD between using GEOS-Chem vertical profile and FLG vertical profile for each size bins are shown in Fig. 8. Their differences are similar to that of the VRAOD with much higher values in the middle troposphere while lower at the surface using the GEOS-Chem vertical profile. Meanwhile, the differences between GEOS-Chem vertical profile and FLG vertical profile for the smallest size bin (0.7 µm) are most significant, and contribute more than 70 % to the differences of total dust VRAOD over the dust source regions (see Fig. 8a). This suggests that more small dust particles are lifted to the middle and upper troposphere, especially over the downwind areas. The clay aerosols (diameter < 2 µm) have lifetimes on the order of a week and produce a strong negative radiative forcing by efficiently scattering shortwave radiation (Kok, 2011). On the other hand, the clear sky thermal IR radiative forcing and cloudy sky TOA solar radiative forcing of dust aerosols are very sensitive to the altitude of the dust and cloud layers (Liao and Seinfeld, 1998). Therefore, the differences of VRAOD produced by small dust particles would undoubtedly result in significant impacts on radiation and heating.

4 Impact of vertical profiles on radiative forcing

The net radiative forcing, ΔF, of solar and IR radiation has been calculated as the change of the net radiation (downward flux, F_{down}, minus upward flux, F_{up}) at the top of atmosphere and at the surface when the dust aerosols are present with respect to the clear air (no dust aerosol) case, according to

$$\Delta F = F_{\text{down}} - F_{\text{up}} \quad (2)$$

$$\text{RF} = \Delta F_{\text{aerosol}} - \Delta F_{\text{clear}}. \quad (3)$$

The daily changes of the AOD and of the aerosol optical properties are not taken into account since the purpose is

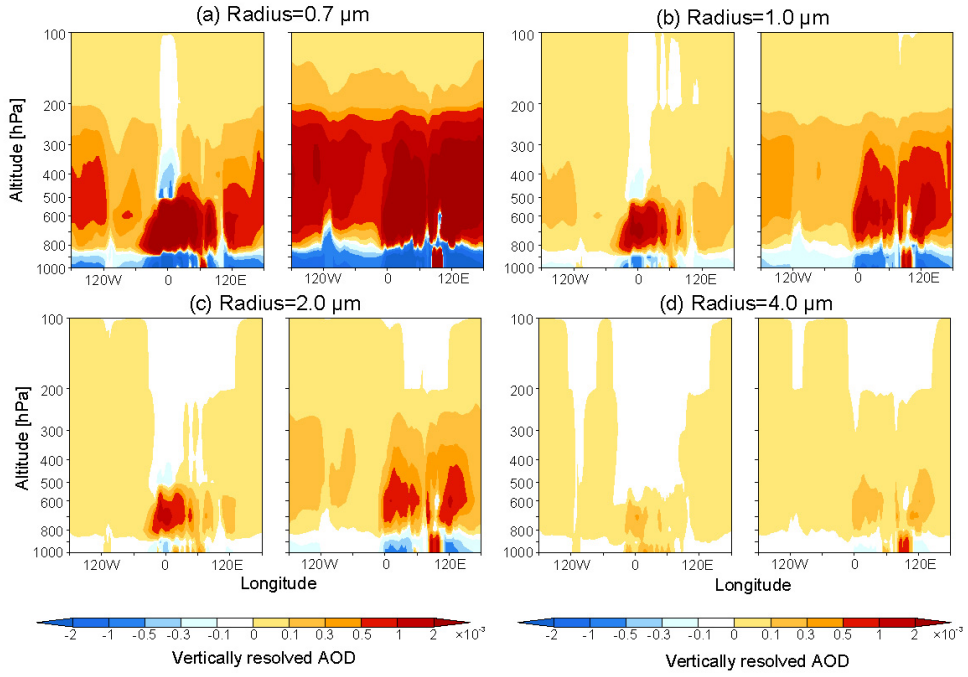

Fig. 8. Differences of dust VRAOD for four size bins **(a)** radii = 0.7 μm; **(b)** radii = 1.0 μm; **(c)** radii = 2.0 μm; **(d)** radii = 4.0 μm between using GEOS-Chem vertical profile and FLG vertical profile (former minus latter) averaged over African dust belt (10–35° N) and Asian dust belt (35–45° N).

to assess the sensitivity of the direct radiative forcing influenced by differences in vertical profile of dust extinction. To examine the radiative forcing in different regions, we focus our analysis on the representations of largest desert in African and Asian source regions, the Sahara desert (10–35° N, 10° W–40° E) and the Gobi desert (40–45° N, 90–110° E), as well as their downwind areas of the Arabian Sea (5–25° N, 60–75° E) and Eastern Asia (35–55° N, 120–150° E).

4.1 Impact of vertical profiles on solar radiative forcing

Table 1 shows the solar and IR radiative forcing at the TOA and at the surface. The solar radiative forcing depends on the surface albedo and properties of the atmospheric column as well as the dust optical properties. Generally, the solar radiative forcing at the TOA is negative for maritime regions since sulfate and small mineral dust particles scatter solar radiation with little absorption produced (Gu et al., 2006). Dust particles also increase the apparent reflectance of the earth over dark surfaces (e.g., ocean); more solar radiation is scattered back to space in the presence of slightly absorbing aerosol. The model predicts a negative solar radiative forcing and exerts cooling effects at the TOA throughout entire atmosphere except with some bright surfaces for both vertical profiles (Fig. 9a, b). The absorption of solar radiation dominates over scattering over bright surfaces (such as snow covered areas), or cloud-covered surfaces, causing a net TOA warming (Weaver et al., 2002). Therefore, the positive values of 0–1 $\mathrm{W\,m^{-2}}$ are shown over the snow areas in high latitude. The positive solar radiative forcing over part of the desert is due to the elevated absorbing dust particles above the highly reflective desert surface (Huang et al., 2009). The solar radiative forcing over both dust source regions and downwind areas exerts significant cooling effect at the TOA. The global mean values of solar radiative forcing at the TOA are $-1.85\,\mathrm{W\,m^{-2}}$ and $-1.73\,\mathrm{W\,m^{-2}}$for the GEOS-Chem vertical profile and FLG vertical profile respectively. The difference in the solar radiative forcing at the TOA between the GEOS-Chem vertical profile and the FLG vertical profile (the former minus later) is shown in Fig. 9c. With the GEOS-Chem vertical profile, the cooling effect is weaker by $0.19\,\mathrm{W\,m^{-2}}$ and $0.24\,\mathrm{W\,m^{-2}}$ over the Sahara and Gobi deserts than that with FLG vertical profile. The FLG vertical profile allows for more dust particles in the upper troposphere over the dust source regions than that of the GEOS-Chem vertical profile (Figs. 7 and 8), which exerts more cooling at the TOA. However, more dust particles, especially the small size particles that mostly scatter solar radiation, are lifted into the middle and upper troposphere over the downwind areas by using the GEOS-Chem vertical profile (Figs. 7 and 8). This results in more reflection at the TOA and much stronger cooling effect over all except Arabian Sea, which shows weaker cooling. A possible reason is that Arabian Sea is located close to the dust source regions of Sahara desert and Arabian Peninsula. Other

Table 1. Solar and IR forcing ($W\,m^{-2}$) at the TOA and at the surface.

	Vertical profile	Solar forcing		IR forcing	
		TOA	Surface	TOA	Surface
Global	GEOS-Chem	−1.85	−3.42	0.20	0.42
	FLG	−1.73	−3.46	0.16	0.46
	Diff	−0.12	0.04	0.04	−0.04
Sahara (10–35° N, 10° W–40° E)	GEOS-Chem	−7.53	−22.32	1.61	5.26
	FLG	−7.74	−22.96	1.78	5.43
	Diff	0.19	0.64	−0.17	−0.17
Gobi (40–45° N, 90–110° E)	GEOS-Chem	−12.24	−27.00	1.90	4.99
	FLG	−12.37	−28.16	1.84	5.36
	Diff	0.24	1.16	0.06	−0.37
Arabian Sea (5–25° N, 60–75° E)	GEOS-Chem	−8.35	−13.47	0.32	1.10
	FLG	−9.04	−14.11	0.46	1.10
	Diff	0.69	0.64	−0.14	0.00
Eastern Asia (35–55° N, 120–150° E)	GEOS-Chem	−7.69	−11.61	0.82	1.00
	FLG	−6.63	−11.49	0.38	1.26
	Diff	−1.06	−0.12	0.44	−0.26

than some far away downwind areas (e.g., Eastern Asian), the vertical structure of dust distribution over Arabian Sea follows that of the African source region (Fig. 5), leading to similar radiative impact (Table 1). The solar radiative forcing is less dependent on the vertical profile for low absorbing particles at the TOA than that of absorbing particles, with up to a 10 % variation in the daily average forcing over the dust source region (Meloni et al., 2005). Here, the differences in averaged solar radiative forcing at the TOA between using GEOS-Chem vertical profile and FLG vertical profile are less than 3 % over the Sahara and Gobi desert. However, the impact of the vertical profile on the solar radiative forcing over the downwind areas is much larger than that over the dust source region. The differences are about 10 % over Arabian Sea and Eastern Asia.

Even though the TOA forcing is often small, the surface forcing can be relatively large, especially over the dust source regions. Both solar absorption and reflection within the atmosphere tend to cool the surface (Fig. 10). The solar radiative forcing at the surface is negative (cooling effect) with a global mean value of $-3.42\,W\,m^{-2}$ for GEOS-Chem vertical profile and $-3.46\,W\,m^{-2}$ for FLG vertical profile (Table 1). It increases significantly to more than $-20\,W\,m^{-2}$ over the dust source regions of Sahara and Gobi deserts, indicating a decrease in the solar insolation at the surface associated with more scattering and absorption of radiation by dust particles. The differences of solar radiative forcing at the surface between GEOS-Chem vertical profile and FLG vertical profile are evident over the dust source regions and their surrounding downwind areas, such as Arabian Sea (Fig. 10c). With the GEOS-Chem vertical profile, there are more solar net flux at the surface (see Fig. 11b), which results in less cooling produced over the Sahara, Gobi and Arabian Sea than that with FLG vertical profile (Table 1).

4.2 Differences of solar radiative forcing over dust source regions and downwind areas

In order to explain the differences in the dust radiative forcing between the dust source regions and downwind areas, two samples were selected to show the impact of the different vertical profiles of dust vertically resolved ADO on the radiative forcing through the atmosphere (see Figs. 11 and 12). One sample is selected from the largest dust source region in the world, the Sahara desert (10° E, 20° N). The other sample is located over the downwind areas of Eastern Asia (140° E, 40° N), which is an important pathway of trans-Pacific transport (Nam et al., 2010). At the TOA, the differences of net radiative forcing between the GEOS-Chem vertical profile and the FLG vertical profile are dominated by the differences of the upward flux since the downward flux is the same at the TOA. The differences in the upward flux at the TOA are positively correlated to the differences of VRAOD in the upper troposphere where less dust particles over the source regions lead to less solar reflection and less upward flux for low absorbing aerosols. Thus, differences in net forcing between the GEOS-Chem vertical profile and the FLG vertical profile at the TOA are found to be positive over the dust source regions (Fig. 11b) and negative over the downwind areas (Fig. 12b). Vertically, the change of downward flux at a certain layer is negatively correlated to the change of VRAOD in that layer. Fewer particles lead to less reflection and absorption, resulting in more downward flux at the bottom of that layer. The

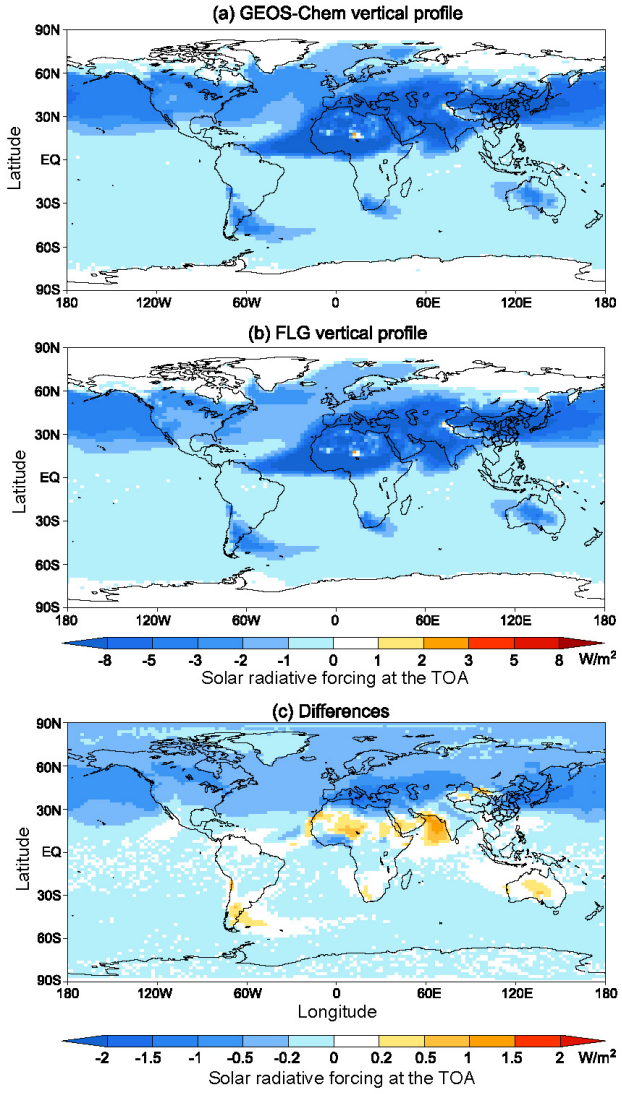

Fig. 9. Solar radiative forcing at the TOA with **(a)** GEOS-Chem vertical profile; **(b)** FLG vertical profile; and **(c)** differences between using GEOS-Chem vertical profile and FLG vertical profile (former minus latter). Unit: W m^{-2}.

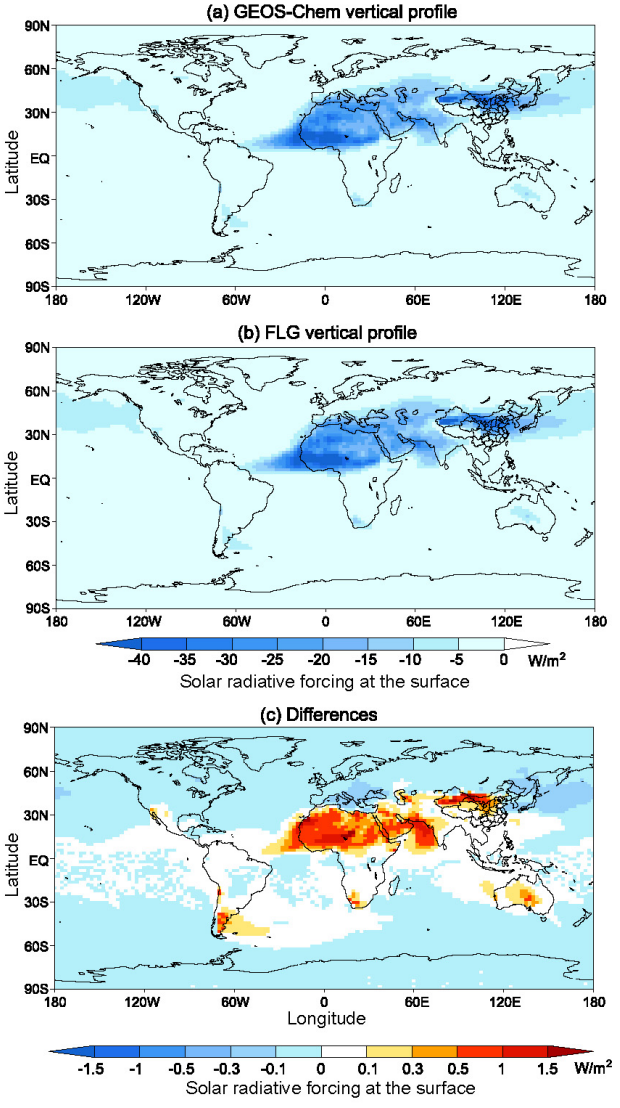

Fig. 10. Solar radiative forcing at the surface with **(a)** GEOS-Chem vertical profile; **(b)** FLG vertical profile; and **(c)** differences between using GEOS-Chem vertical profile and FLG vertical profile (former minus latter). Unit: W m^{-2}.

change of upward flux is normally proportional to the change of downward flux, where more downward flux leads to more upward flux. When the vertical change of extinction is positive/negative, the corresponding differences in net flux will be decreasing/increasing. Smaller VRAOD above 600 hPa with GEOS-Chem vertical profile over the dust source region (Fig. 11a) leads to an increasing downward flux from the TOA to 600 hPa (Fig. 11b). Therefore, the differences of net radiative forcing between the GEOS-Chem vertical profile and the FLG vertical profile exert an increasing trend. More dust particles are seen at 600–800 hPa by using the GEOS-Chem vertical profile, which increases both scattering and absorption of solar radiation, leading to a decreasing trend for downward flux at 700–800 hPa due to the reduction of available radiation. The positive differences in net radiative forcing are due the magnitude of the much larger differences in downward flux. Over the downwind areas, though the dust VRAOD are quite different to those over source region, the results are similar. The differences of net radiative forcing between GEOS-Chem and FLG vertical profiles show decreasing and negative values above 700 hPa (Fig. 12b) since the dust VRAOD is much larger using the GEOS-Chem profile above that altitude (Fig. 12a). The impact of vertical profiles on solar radiative forcing at the surface is more complicated relative to that at the TOA since it depends on not only

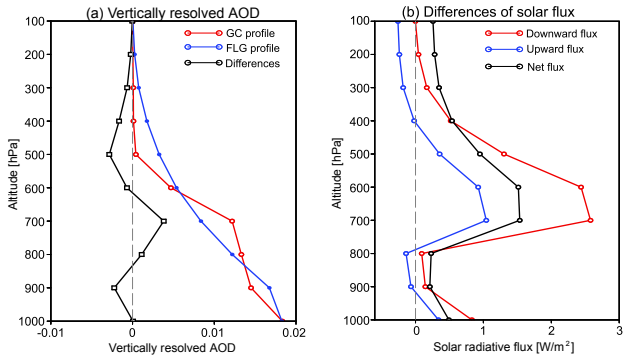

Fig. 11. Vertical profiles of **(a)** dust extinction and **(b)** the differences of dust solar radiative flux [W m^{-2}] at the location of Sahara desert (10° E, 20° N).

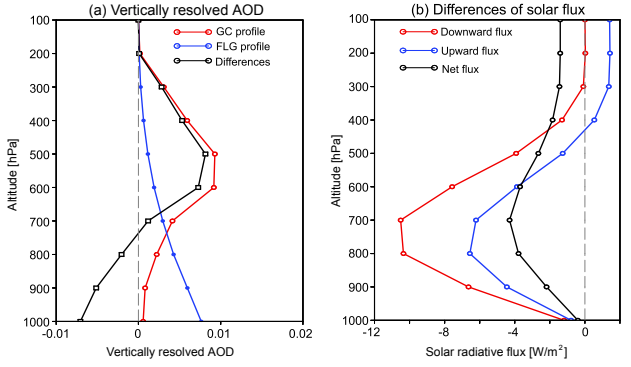

Fig. 12. Same as Fig. 11, but at the location of Eastern Asia (140° E, 40° N).

the available downward radiation throughout the atmospheric column, but also the upward flux at the surface.

4.3 Impact of vertical profiles on IR radiative forcing

In addition to the solar radiative forcing, as one of the absorbing aerosols, dust particles also exert a significant thermal IR radiative forcing, thus contributing to the greenhouse effect (Haywood et al., 2005; Gu et al., 2006; Shell et al., 2007). The definition of IR radiative forcing is equivalent to that of the solar radiative forcing (see Eqs. 2–3), the difference between irradiances with and without aerosol at the TOA and surface. Normally, the IR radiative forcing is effective for the full 24 h and is a strong function of the surface temperature (Haywood et al., 2005). Dust particles have a warming effect at the TOA for IR radiation for both the GEOS-Chem and FLG vertical profiles over the African and Asian dust source regions and their downwind areas (Fig. 13). The average IR radiative forcing over the Saharan desert is about 1.6 W m^{-2} and 1.8 W m^{-2} at the TOA for the GEOS-Chem FLG vertical profiles, respectively. This warming effect at the TOA is also dependent on the size of the dust particles (Gu et al., 2006).

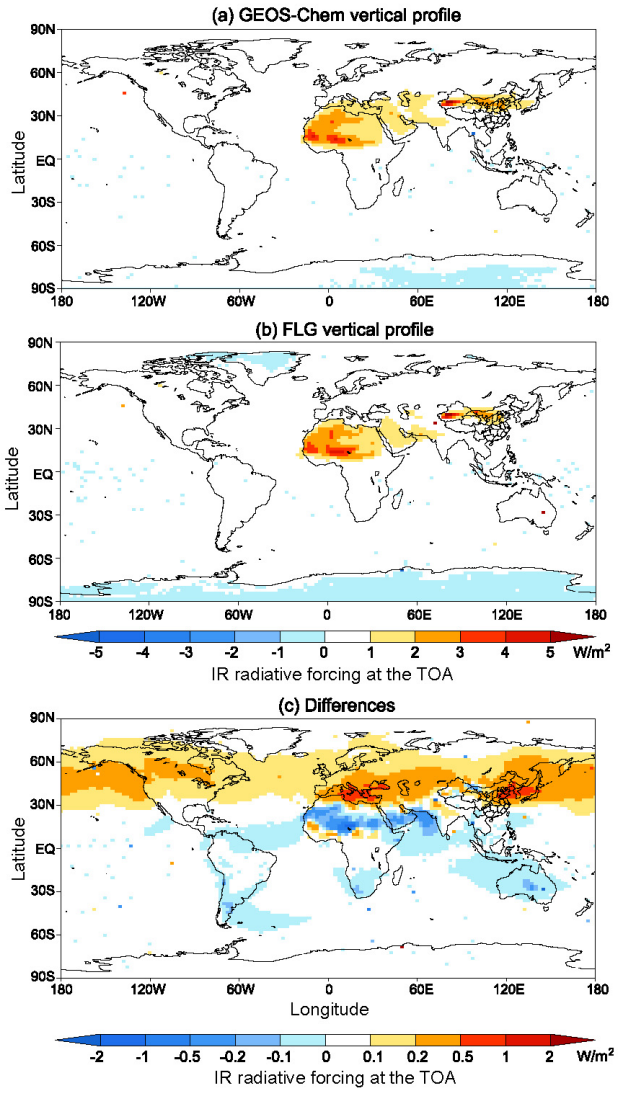

Fig. 13. IR radiative forcing at the TOA with **(a)** GEOS-Chem vertical profile; **(b)** FLG vertical profile; and **(c)** differences between using GEOS-Chem vertical profile and FLG vertical profile (former minus latter). Unit: W m^{-2}.

The IR radiation interacts more efficiently with larger particles, while the solar radiation interacts more efficiently with smaller particles (Yoshioka et al., 2007). Therefore, the IR forcing is highest near-dust source regions where more large dust particles are present since larger particles have shorter lifetimes and travel shorter distances (Kok et al., 2011).

The differences in IR forcing between the GEOS-Chem vertical profile and the FLG vertical profile at the TOA are apparent. Since there are less large dust particles in the middle and upper troposphere when using the GEOS-Chem vertical profile, the IR forcing is lower by 0.17 W m^{-2} and 0.14 W m^{-2} by using GEOS-Chem vertical profile than that using the FLG vertical profile over both Saharan desert and the Arabian Sea (Fig. 13c). However, the warming effect with

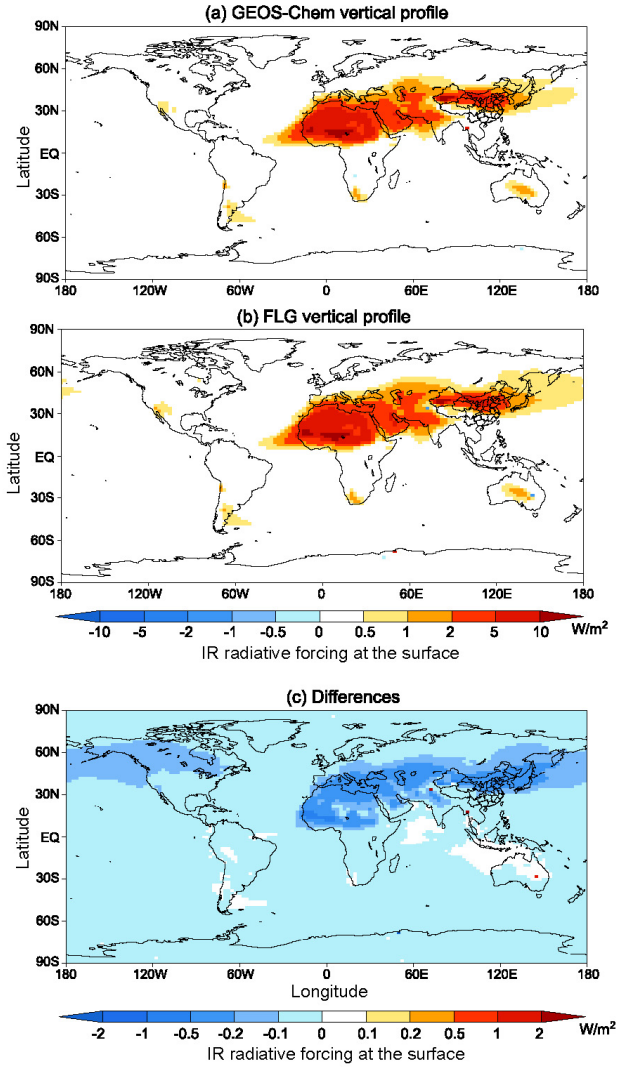

Fig. 14. IR radiative forcing at the surface with **(a)** GEOS-Chem vertical profile; **(b)** FLG vertical profile; and **(c)** differences between using GEOS-Chem vertical profile and FLG vertical profile (former minus latter). Unit: $\mathrm{W\,m^{-2}}$.

GEOS-Chem vertical profile is $0.44\,\mathrm{W\,m^{-2}}$ and $0.06\,\mathrm{W\,m^{-2}}$ higher than that of FLG vertical profile over the downwind area of the Eastern Asia and Asian source region (Gobi desert) due to more dust particles in the free troposphere (see Figs. 7 and 8). At the surface, the IR forcing is smaller than the solar forcing over the dust source regions (Fig. 14). Dust absorption reduces the reemission at the top of the atmosphere and increases the downward irradiance at the surface, leading to a positive IR radiative forcing and warming at the surface. The warming effect of IR radiation is much smaller globally by using the GEOS-Chem vertical profile at the surface.

While an increased IR warming (due to the dust "greenhouse effect") somewhat balances the cooling, the net result is typically negative (Shell et al., 2007). The global average net forcing is dominated by the solar forcing with a cooling effect at the TOA and at the surface for both the GEOS-Chem vertical profile and the FLG vertical profile. The net cooling is about $-17.0\,\mathrm{W\,m^{-2}}$ over the Sahara desert and $-22.0\,\mathrm{W\,m^{-2}}$ over the Gobi desert by using the GEOS-Chem vertical profile. The net forcing at the surface over Eastern Asia is $-10.6\,\mathrm{W\,m^{-2}}$ with the GEOS-Chem vertical profile, which exerts more significant cooling than that of using FLG vertical profile.

5 Impact of vertical profiles on heating rate

Dust particles not only scatter but also absorb solar and IR radiation, which can influence the heating profiles and contribute to large diabatic heating in the atmosphere (Fu et al., 1997; Huang et al., 2006). Model studies show that an elevated Saharan dust layer can change the atmospheric heating rate significantly (Carlson and Benjamin, 1980). The GEOS-Chem coupled FLG-RTM is used here to calculate the solar and IR dust heating rate based on GEOS-Chem vertical profile and FLG vertical profiles.

Figures 15–17 show the impact of dust particles on the solar, IR, and net heating rates over the two dust belts by using GEOS-Chem vertical profile and FLG vertical profile, respectively. They are calculated as the differences between the simulated radiative heating rates with and without the dust particles. The pattern of the solar heating rate is consistent with that of the dust VRAOD due to the absorption of solar radiation by dust. Dust particles heat the atmosphere by more than $0.5\,\mathrm{K\,day^{-1}}$ over African and Asian source regions for both using GEOS-Chem and FLG profiles (Fig. 15a, b), but there is slight cooling effect near the surface over the non-dust source regions by using GEOS-Chem vertical profile. The solar heating rate shows a maximum corresponding to that of the high dust VRAOD. The differences of the heating rates between GEOS-Chem vertical profile and FLG vertical profile (Fig. 15c) are consistent with the differences of their VRAOD (Fig. 7). The maximum of the difference is shown at 700 hPa over the African dust source region. Although dust particles exert less effect on IR radiative heating rates with very small values (Fig. 16), they do show a warming effect near surface over the non-dust source regions while significant cooling effect in the low and middle troposphere over the dust source regions. The IR cooling ranges from 0.06 $\mathrm{K\,day^{-1}}$ to 0.08 $\mathrm{K\,day^{-1}}$, which partly compensates the large solar radiative heating near the dust layers. Fig. 17 shows the net heating by using the GEOS-Chem and the FLG vertical profiles over the two dust belts. The vertical distribution of net radiative heating is similar to that of the dust VRAOD. The maximum radiative net heating rate is consistent with the distribution of highest VRAOD. The net dust heating at the dust layer is about $0.2\,\mathrm{K\,day^{-1}}$ to $0.5\,\mathrm{K\,day^{-1}}$ over the dust source regions for both vertical profiles. The dust

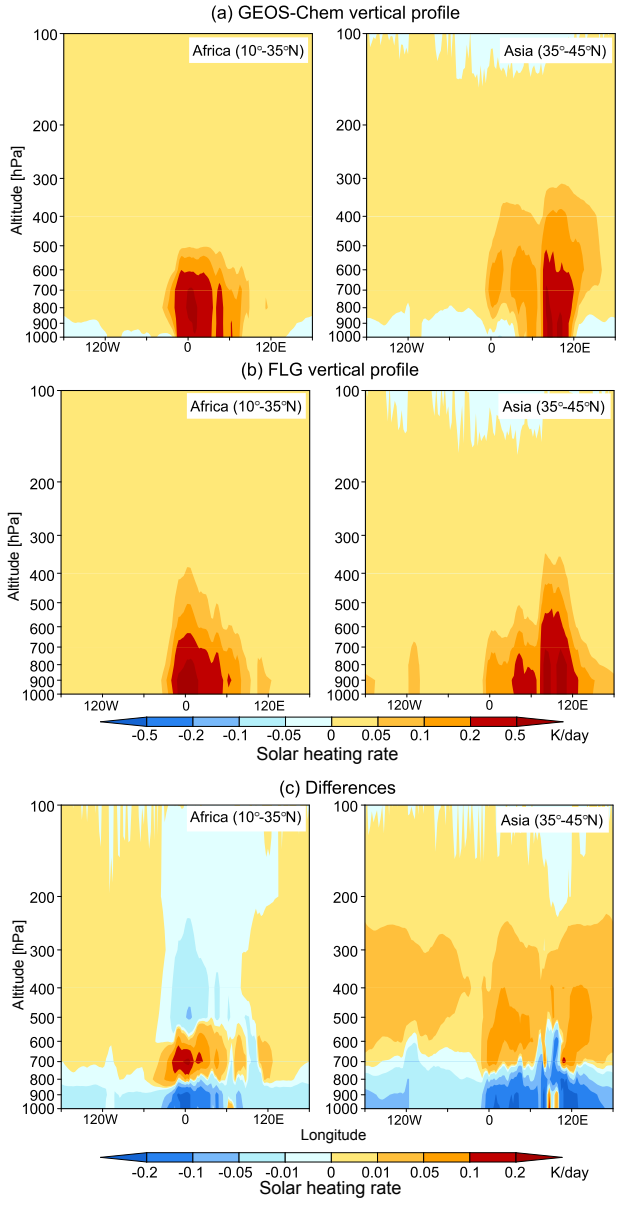

Fig. 15. Altitude–longitude cross sections of solar heating rate due to dust with **(a)** GEOS-Chem vertical profile; **(b)** FLG vertical profile; and **(c)** differences between using GEOS-Chem vertical profile and FLG vertical profile (former minus latter) averaged over African dust belt (10–35° N) and Asian dust belt (35–45° N). Unit: K.

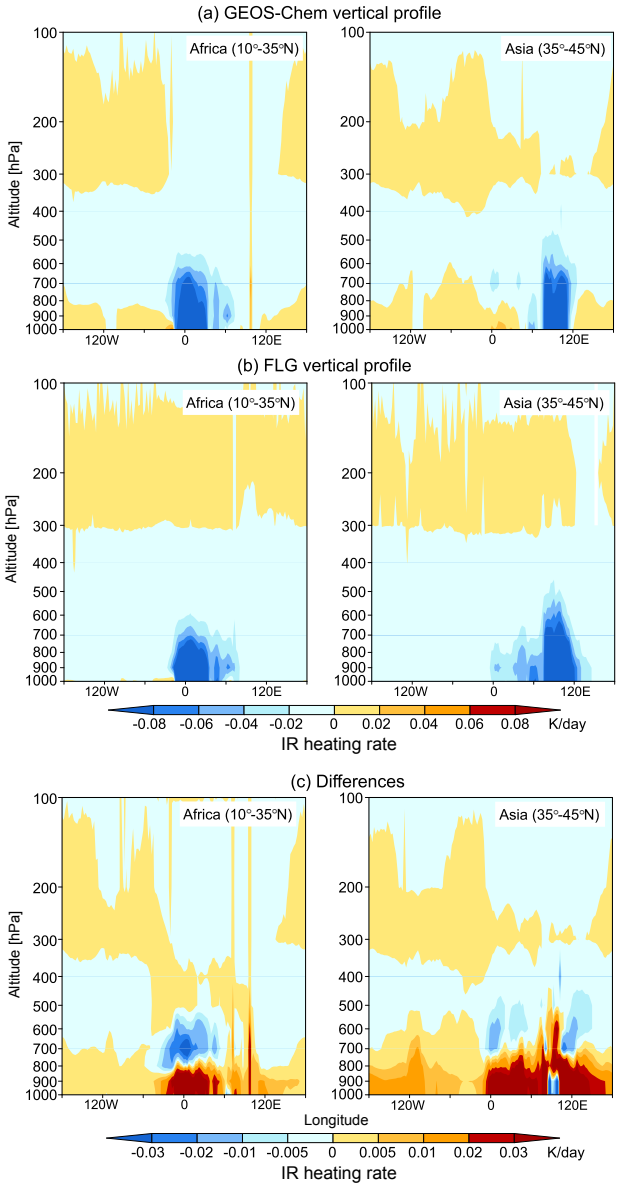

Fig. 16. Same as Fig. 15, but for IR heating rate due to dust.

radiative net heating based on GEOS-Chem vertical profile reflects the impact of transport. The net heating rate due to the dust particles are less than 0.05 K day^{-1} above the dust layer and the non-dust source regions. The differences of the net heating rate between using GEOS-Chem vertical profile and FLG vertical profile are the same as those of the solar heating rate (Figs. 15c and 17c) since the net heating rate is dominated by the solar heating rate (Huang et al., 2009).

An enhanced net heating rate is evident in the middle and upper troposphere over African and Asian source regions by using GEOS-Chem vertical profile, but it is much smaller by 0.1 K day^{-1} near-surface layers compare to using FLG vertical profile (Fig. 17c). Obviously, the radiative net heating is sensitive to the dust VRAOD, which may play an important role in modulating regional circulation.

6 Summary and discussion

The global dust emission in the GEOS-Chem global 3-D CTM has been constrained using MISR AOD. Using the adjusted emission, the simulations of daily surface $PM_{2.5}$

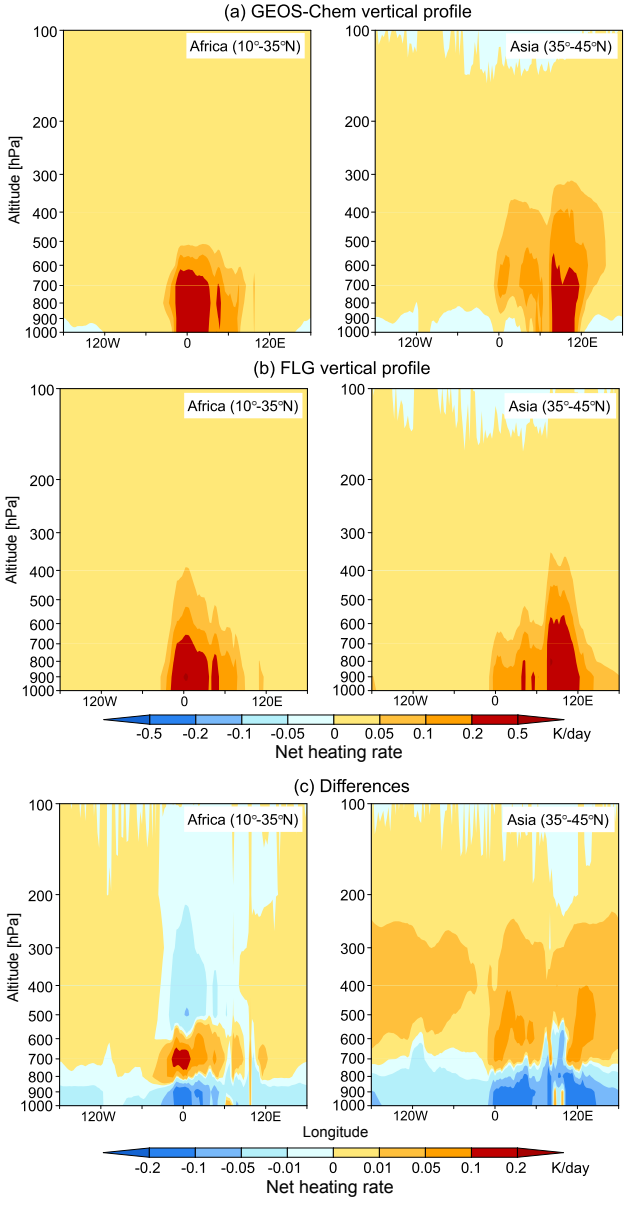

Fig. 17. Same as Fig. 15, but for net heating rate due to dust.

dust concentration were improved over the western coastal US where the dust was mainly influenced by the long-range transport from Asian and African source regions (VanCuren and Cahill, 2002; Yu et al., 2012; Zhang et al., 2013). Significantly positive biases of simulated dust AOD over source regions compared to the MISR observations have also been corrected. The simulated vertical structure of dust extinction is consistent with that of CALIPSO measurement. With this more realistic simulation of dust concentration and AOD, the GEOS-Chem chemical transport model was coupled with the FLG spectral radiative transfer model to investigate the sensitivities of radiative forcing to dust vertical profiles. The calculations of solar and infrared radiation at the TOA and the surface are based on the more realistic vertical profile of extinction simulated by GEOS-Chem and the prescribed "climatological" FLG profile of extinction to actually quantify their discrepancies. The calculation is sensitivity study only based on April 2006, which is not comparable to global climatological estimates. Using the GEOS-Chem profile reflected the differences of extinction between dust and non-dust source regions, while using FLG vertical profile shows a consistent pattern of VRAOD both in dust and non-dust source regions. The dust VRAOD was consistently higher from the surface to 600 hPa over the African and Asian dust source regions; it then decreased with increasing altitude when using the GEOS-Chem vertical profile. The largest VRAOD was in the middle troposphere second only to the surface for non-dust source regions (along the downwind areas).

The coupled calculations involving GEOS-Chem and FLG-RTM with more realistic dust vertical profile minimized the physical inconsistencies between the 3-D CTM aerosol fields and the radiative transfer calculations and contribute directly to the evaluation of dust heating rate and radiative forcing. The global mean radiative forcing was negative in the solar part of the spectrum both at the TOA and at the surface, associated with the predominantly scattering nature of dust particles at these wavelengths. However, the vertical distributions of dust particles strongly affected the estimated radiative forcing at the TOA and the surface. The global negative radiative forcings were enhanced 7 % at the TOA and reduced 1.2 % at the surface using GEOS-Chem vertical profile compared to using FLG vertical profile. It also reduced solar radiative forcing by about 0.2–0.25 W m^{-2} at the TOA over the African and Asia dust source regions. Over the downwind areas, there were about 16 % enhancements of radiative forcings at the TOA while 1 % reduction at the surface over Eastern Asia by using GEOS-Chem vertical profile, as compared to FLG vertical profile. The differences of radiative forcing at the TOA were mainly dominated by the upward solar flux, wherever fewer (more) dust particles would result in less (more) solar reflection and less (more) upward flux for low absorbing aerosols. The thermal infrared radiative forcing at the TOA was more sensitive to dust vertical profile than that of solar radiative forcing. More then 100 % increase of thermal infrared radiative forcing was indicated at the surface over Eastern Asia, while about 30 % reduction over Arabian Sea.

The differences of dust vertical profile not only impacted on the radiative forcing, but also changed the atmospheric heating rate. The largest solar heating rate was consistent with the maximum of dust VRAOD due to the absorption by dust particles. The radiative net heating dominated by the solar heating rate is also sensitive to different vertical profiles and shows substantial differences between the GEOS-Chem vertical profile and the FLG vertical profile. The net heating rate is much larger in the middle and upper troposphere over the African and Asian source regions, while smaller

near-surface layers when using the GEOS-Chem vertical profile. Chen et al., (2010) found that the warming effect due to dusty air between 750 and 550 hPa resulted in an increase of the vertical wind shear to the south of SAL, where easterly wave disturbances and tropical storms usually occur. This enhanced net heating rate plays an important role in warming the middle atmosphere, especially over the dust source regions of SAL where the enhancement of the vertical wind shear in this layer could potentially impact on the tropical cyclones genesis and development (Pratt and Evans, 2009). Using a more realistic vertical profile simulated by GEOS-Chem would improve not only the estimate of dust radiative forcing and heating rate but also the understanding of modulating regional circulation.

Acknowledgements. We would like to thank the editor and the reviewers for the helpful comments. Y. Gu was supported by NSF Grant ATM-0924876. The CALIPSO data were obtained from the NASA Langley Research Center Atmospheric Science Data Center.

Edited by: J. Quaas

References

Alexander, B., Savarino, J., Lee, C. C. W., Park, R. J., Jacob, D. J., Thiemens, M. H., Li, Q. B., and Yantosca, R. M.: Sulfate formation in sea-salt aerosols: Constraints from oxygen isotopes, J. Geophys. Res., 110, D10307, doi:10.1029/2004JD005659, 2005.

Andreae, M. O.: Climatic effects of changing atmospheric aerosol levels, in Future Climates of the World: A Modelling Perspective, World Survey of Climatology, vol. 16, edited by A. Henderson-Sellers, 347–398, Elsevier, New York, 1995.

Bey, I., Jacob, D. J., Yantosca, R. M., Logan, J. A., Field, B. D., Fiore, A. M., Li, Q. B., Liu, H. G. Y., Mickley, L. J., and Schultz, M. G.: Global modeling of tropospheric chemistry with assimilated meteorology: Model description and evaluation, J. Geophys. Res., 106, 23073–23096, 2001.

Bou Karam, D., Flamant, C., Knippertz, P., Reitebuch, O., Pelon, J., Chong, M., and Dabas, A.: Dust emissions over the Sahel associated with the West African monsoon intertropical discontinuity region: A representative case study, Q. J. Roy. Meteorol. Soc., 134, 621–634, doi:10.1002/qj.244, 2008.

Carlson, T. N. and Benjamin, S. G.: Radiative heating rates for Saharan dust, J. Atmos. Sci., 37, 193–213, 1980.

Carlson, T. N. and Prospero, J. M.: The large-scale movement of Saharan air outbreaks over the equatorial North Atlantic, J. Appl. Meteorol., 11, 283, 1972.

Charlock, T. P., Rose, F. G., Rutan, D., Jin, Z., Fillmore, D., and Collins, W.: Global retrieval of the surface and atmospheric radiation budget and direct aerosol forcing, paper presented at Conference on Satellite Meteorology, p. 8.11, Am. Meteorol. Soc., Norfolk, VA, 2004.

Chaudhry, Z., Martins, J. V., Li, Z., Tsay, S.-C., Chen, H., Wang, P., Wen, T., Li, C., and Dickerson, R. R.: In situ measurements of aerosol mass concentration and radiative properties in Xianghe, southeast of Beijing, J. Geophys. Res., 112, D23S90, doi:10.1029/2007JD009055, 2007.

Chen, S.-H., Wang, S.-H., and Waylonis, M.: Modification of Saharan air layer and environmental shear over the eastern Atlantic Ocean by dust-radiation effects, J. Geophys. Res., 115, D21202, doi:10.1029/2010JD014158, 2010.

Chin, M., Chu, A., Levy, R., Remer, L., Kaufman, Y., Holben, B., Eck, T., Ginoux, P., and Gao, Q. Aerosol distribution in the Northern Hemisphere during ACE-Asia: results from global model, satellite observations, and Sun photometer measurements, J. Geophys. Res., 109, D23S90, doi:10.1029/2004JD004829, 2004.

Chu, D. A., Kaufman, Y. J., Ichoku, C., Remer, L. A., Tanre, D., and Holben, B. N.: Validation of MODIS aerosol optical depth retrieval over land, Geophys. Res. Lett., 29, 8007, doi:10.1029/2001GL013205, 2002.

Colarco, P. R., Toon, O. B., Torres, O., and Rasch, F. J.: Determining the UV imaginary part of refractive index of Saharan dust particles from TOMS data and a three dimensional model of dust transport, J. Geophys. Res., 107, 4289, doi:10.1029/2001JD000903, 2002.

d'Almeida, G. A., Koepke, P., and Shettle, E. P.: Atmospheric Aerosols—Global Climatology and Radiative Characteristics, 561 pp., A. Deepak, Hampton, Va, 1991.

de Rooij, W. A. and van der Stap, C. C. A. H. : Expansion of Mie scattering matrics in generalized spherical functions, Astron. Astrophys., 131, 237–248, 1984.

Elterman, L.: UV, visible and IR attenuation for altitudes to 50 km, Rep. AFCR-68-0153, Air Force Cambridge Res. Lab., Bedford, Mass., 1968.

Fairlie, T. D., Jacob, D. J., and Park, R. J., The impact of transpacific transport of mineral dust in the United States, Atmos. Environ., 41, 1251–1266, 2007.

Fairlie, T. D., Jacob, D. J., Dibb, J. E., Alexander, B., Avery, M. A., van Donkelaar, A., and Zhang, L.: Impact of mineral dust on nitrate, sulfate, and ozone in transpacific Asian pollution plumes, Atmos. Chem. Phys., 10, 3999–4012, doi:10.5194/acp-10-3999-2010, 2010.

Fu, Q. and Liou, K. N.: On the correlated k-distribution method for radiative transfer in nonhomogeneous atmospheres, J. Atmos. Sci., 49, 2139–2156, 1992.

Fu, Q. and Liou, K. N.: Parameterization of the radiative properties of cirrus clouds, J. Atmos. Sci., 50, 2008–2025, 1993.

Fu, Q., Liou, K. N., Cribb, M. C., Charlock, T. P., and Grossman, A.: Multiple scattering parameterization in thermal infrared radiative transfer, J. Atmos. Sci., 54, 2799–2812, 1997.

Gadhavi, H. and Jayaraman, A.: Airborne lidar study of the vertical distribution of aerosols over Hyderabad, an urban site in central India, and its implication for radiative forcing calculations, Ann. Geophys., 24, 2461–2470, doi:10.5194/angeo-24-2461-2006, 2006.

Generoso, S., Bey, I., Labonne, M., and Bréon, F.-M.: Aerosol vertical distribution in dust outflow over the Atlantic: Comparisons between GEOS-Chem and Cloud-Aerosol Lidar and Infrared Pathfinder Satellite Observation (CALIPSO), J. Geophys. Res., 113, D24209, doi:10.1029/2008JD010154, 2008.

Ginoux, P., Chin, M., Tegen, I., Prospero, J. M., Holben, B., Dubovik, O., and Lin, S.-J.: Sources and distributions of dust aerosols simulated with the GOCART model, J. Geophys. Res., 106, 20255–20274, 2001.

Ginoux, P., Prospero, J. M., Torres, O., and Chin, M.: Long-term simulation of global dust distribution with the GOCART model: correlation with North Atlantic oscillation, Environ. Model. Softw., 19, 113–128, 2004.

Gu, Y., Farrara, J., Liou, K. N., and Mechoso, C. R.: Parameterization of cloud-radiation processes in the UCLA general circulation model, J. Climate, 16, 3357–3370, 2003.

Gu, Y., Liou, K. N., Xue, Y., Mechoso, C. R., Li, W., and Luo, Y.: Climatic effects of different aerosol types in China simulated by the University of California, Los Angeles atmospheric general circulation model, J. Geophys. Res., 111, D15201, doi:10.1029/2005JD006312, 2006.

Gu, Y., Liou, K. N., Chen, W., and Liao, H.: Direct climate effect of black carbon in China and its impact on dust storms, J. Geophys. Res., 115, D00K14, doi:10.1029/2009JD013427, 2010.

Gu, Y., Liou, K. N., Ou, S. C., and Fovell, R.: Cirrus cloud simulations using WRF with improved radiation parameterization and increased vertical resolution, J. Geophys. Res., 116, D06119, doi:10.1029/2010JD014574, 2011.

Hamonou, E., Chazette, P., Balis, D., Dulac, F., Schneider, X., Galani, E., Ancellet, G., and Papayannis, A.: Characterization of the vertical structure of Saharan dust export to the Mediterranean basin, J. Geophys. Res., 104, 22257–22270, doi:10.1029/1999JD900257, 1999.

Haywood, J. M., Ramaswamy, V., and Soden, B. J.: Tropospheric aerosol climate forcing in clear-sky satellite observations over the oceans, Science, 283, 1299–1305, 1999.

Haywood, J. M., Allan, R. P., Culverwell, I., Slingo, T., Milton, S., Edwards, J., and Clerbaux, N.: Can desert dust explain the outgoing longwave radiation anomaly over the Sahara during July 2003?, J. Geophys. Res., 110, D05105, doi:10.1029/2004JD005232, 2005.

Hess, M., Koepke, P., and Schult, I.: Optical properties of aerosols and clouds: The software package OPAC, B. Am. Meteorol. Soc., 79, 831–844, 1998.

Huang, J., Lin, B., Minnis, P., Wang, T., Wang, X., Hu, Y., Yi, Y., and Ayers, J. K.: Satellite-based assessment of possible dust aerosols semidirect effect on cloud water path over East Asia, Geophys. Res. Lett., 33, L19802, doi:10.1029/2006GL026561, 2006.

Huang, J., Fu, Q., Su, J., Tang, Q., Minnis, P., Hu, Y., Yi, Y., and Zhao, Q.: Taklimakan dust aerosol radiative heating derived from CALIPSO observations using the Fu-Liou radiation model with CERES constraints, Atmos. Chem. Phys., 9, 4011–4021, doi:10.5194/acp-9-4011-2009, 2009.

Huebert, B. J., Howell, S. G., Zhuang, L., Heath, J. A., Litchy, M. R., Wylie, D. J., Kreidler-Moss, J. L., Cöppicus, S., and Pfeiffer, J. E.: Filter and impactor measurements of anions and cations during the First Aerosol Characterization Experiment (ACE 1), J. Geophys. Res., 103, 16493–16509, 1998.

Intergovernmental Panel on Climate Change: The Physical Science Basis. Contribution of Working Group I to the Fourth Assessment Report of the Intergovernmental Panel on Climate Change, edited by: Solomon, S., Qin, D., Manning, M., Chen, Z., Marquis, M., Averyt, K. B., Tignor, M., and Miller, H. L., Cambridge Univ. Press, Cambridge, UK, 2007.

Johnson, B. T., Heese, B., McFarlane, S. A., Chazette, P., Jones, A., and Bellouin, N.: Vertical distribution and radiative effects of mineral dust and biomass burning aerosol over West Africa during DABEX, J. Geophys. Res., 113, D00C12, doi:10.1029/2008JD009848, 2008.

Johnson, M. S., Meskhidze, N., and Kiliyanpilakkil, V. P.: A global comparison of GEOS-Chem-predicted and remotely-sensed mineral dust aerosol optical depth and extinction profiles, J. Adv. Model. Earth Syst., 4, M07001, doi:10.1029/2011MS000109, 2012.

Kahn, R. A., Gaitley, B. J., Martonchik, J. V., Diner, D. J., and Crean, K. A.: Multiangle Imaging Spectroradiometer (MISR) global aerosol optical depth validation based on 2 years of coincident Aerosol Robotic Network (AERONET) observations, J. Geophys. Res., 110, D10S04, doi:10.1029/2004JD004706, 2005.

Karyampudi, V. M., Palm, S. P., Reagen, J. A., Fang, H., Grant, W. B., Hoff, R. M., Moulin, C., Pierce, H. F., Torres, O., Browell, E. V., and Melfi, S. H.: Validation of the Saharan dust plume conceptual model using lidar, Meteosat, and ECMWF data, B. Am. Meteorol. Soc., 80, 1045–1075, 1999.

Knippertz, P. and Todd, M. C.: The central west Saharan dust hot spot and its relation to African easterly waves and extratropical disturbances, J. Geophys. Res., 115, D12117, doi:10.1029/2009JD012819, 2010.

Knippertz, P. and Todd M. C.: Mineral dust aerosols over the Sahara: Meteorological controls on emission and transport and implications for modeling, Rev. Geophys., 50, RG1007, doi:10.1029/2011RG000362, 2012.

Koch, J. and Renno, N. O.: The role of convective plumes and vortices on the global aerosol budget, Geophys. Res. Lett., 32, L18806, doi:10.1029/2005GL023420, 2005.

Koffi, B., Schulz, M., Bréon, F.-M., Griesfeller, J., Winker, D., Balkanski, Y., Bauer, S., Berntsen, T., Chin, M., Collins, W. D., Dentener, F., Diehl, T., Easter, R., Ghan, S., Ginoux, P., Gong, S., Horowitz, L. W., Iversen, T., Kirkevåg, A., Koch, D., Krol, M., Myhre, G., Stier, P., and Takemura, T.: Application of the CALIOP layer product to evaluate the vertical distribution of aerosols estimated by global models: AeroCom phase I results, J. Geophys. Res., 117, D10201, doi:10.1029/2011JD016858, 2012.

Kok, J. F.: A scaling theory for the size distribution of emitted dust aerosols suggests climate models underestimate the size of the global dust cycle, P. Natl. Acad. Sci., 108, 1016–1021, 2011.

Lee, C., Martin, R. V., van Donkelaar, A., O'Byrne, G., Krotkov, N., Richter, A., Huey, L. G., and Holloway, J. S.: Retrieval of vertical columns of sulfur dioxide from SCIAMACHY and OMI: Air mass factor algorithm development, validation, and error analysis, J. Geophys. Res., 114, D22303, doi:10.1029/2009JD012123, 2009.

Léon, J. F., Chazette, P., Pelon, J., Dulac, F., and Randriamiarisoa, H.: Aerosol direct radiative impact over the INDOEX area based on passive and active remote sensing, J. Geophys. Res., 107, doi:10.1029/2000JD000116, 2006.

Li, X., Maring, H., Savoie, D., Voss, K., and Prospero, J. M., Dominance of mineral dust in aerosol light scattering in the North Atlantic trade winds, Nature, 380, 416–419, 1996.

Li, Z., Li, C., Chen, H., Tsay, S.-C., Holben, B., Huang, J., Li, B., Maring, H., Qian, Y., Shi, G., Xia, X., Yin, Y., Zheng, Y., and Zhuang, G.: East Asian Studies of Tropospheric Aerosols and their Impact on Regional Climate (EASTAIRC): An overview, J. Geophys. Res., 116, D00K34, doi:10.1029/2010JD015257, 2011.

Liao, H. and Seinfeld, J. H., Radiative forcing by mineral dust aerosols: sensitivity to key variables, J. Geophys. Res., 103, 31637–31645, 1998.

Liou, K. N., Fu, Q., and Ackerman, T. P.: A simple formulation of the delta-four-stream approximation for radiative transfer parameterizations, J. Atmos. Sci., 45, 1940–1947, 1988.

Liu, H., Jacob, D. J., Bey, I., and Yantosca, R. M.: Constraints from 210Pb and 7Be on wet deposition and transport in a global three-dimensional chemical tracer model driven by assimilated meteorological fields, J. Geophys. Res., 106, 12109–12128, 2001.

Maring, H., Savioe, D. L., Izaguirre, M. A., Custals, L., and Reid, J. S.: Vertical distributions of dust and sea-salt aerosols over Puerto Rico during PRIDE measured from a light aircraft, J. Geophys. Res., 108, 8587, doi:10.1029/2002JD002544, 2003.

Martin, R. V., Jacob, D. J., Yantosca, R. M., Chin, M., and Ginoux, P.: Global and regional decreases in tropospheric oxidants from photochemical effects of aerosols, J. Geophys. Res., 108, 4097, doi:10.1029/2002JD002622, 2003.

Martonchik, J. V., Diner, D. J., Kahn, R., Gaitley, B., and Holben, B. N.: Comparison of MISR and AERONET aerosol optical depths over desert sites, Geophys. Res. Lett., 31, L16102, doi:10.1029/2004GL019807, 2004.

McComiskey, A., Schwartz, S. E., Schmid, B., Guan, H., Lewis, E. R., Ricchiazzi, P., and Ogren, J. A.: Direct aerosol forcing: Calculation from observables and sensitivities to inputs, J. Geophys. Res., 113, D09202, doi:10.1029/2007JD009170, 2008.

McFarquhar, G. M. and Wang, H. L.: Effects of aerosols on trade wind cumuli over the Indian Ocean: Model simulations, Q. J. Roy. Meteorol. Soc., 132, 821–843, 2006.

McKendry, I. G., Strawbridge, K. B., O'Neill, N. T., Macdonald, A. M., Liu, P. S. K., Leaitch, W. R., Anlauf, K. G., Jaegle, L., Fairlie, T. D., and Westphal, D. L.: Trans-Pacific transport of Saharan dust to western North America: a case study, J. Geophys. Res., 112, D01103, doi:10.1029/2006JD007129, 2007.

Meloni, D., Sarra, A. D., Iotio, T. D., and Fiocco, G.: Influence of the vertical profile of Saharan dust on the visible direct radiative forcing, J. Quant. Spectrosc. Ra., 93, 497–413, 2005.

Miller, R. L., Cakmur, R. V., Perlwitz, J., Geogdzhayev, I. V., Ginoux, P., Koch, D., Kohfeld, K. E., Prigent, C., Ruedy, R., Schmidt, G. A., and Tegen, I.: Mineral dust aerosols in the NASA Goddard Institute for Space Sciences ModelE atmospheric general circulation model, J. Geophys. Res., 111, D06208, doi:10.1029/2005JD005796, 2006.

Mishchenko, M. I., Dlugach, J. M., Yanovitskij, E. G., and Zakharova, N. T.: Bidirectional reflectance of flat, optically thick particulate layers: An efficient radiative transfer solution and applications to snow and soil surfaces, J. Quant. Spectrosc. Ra., 63, 409–432, doi:10.1016/S0022-4073(99)00028-X, 1999.

Myhre, G., Samset, B. H., Schulz, M., Balkanski, Y., Bauer, S., Berntsen, T. K., Bian, H., Bellouin, N., Chin, M., Diehl, T., Easter, R. C., Feichter, J., Ghan, S. J., Hauglustaine, D., Iversen, T., Kinne, S., Kirkevåg, A., Lamarque, J.-F., Lin, G., Liu, X., Lund, M. T., Luo, G., Ma, X., van Noije, T., Penner, J. E., Rasch, P. J., Ruiz, A., Seland, Ø., Skeie, R. B., Stier, P., Takemura, T., Tsigaridis, K., Wang, P., Wang, Z., Xu, L., Yu, H., Yu, F., Yoon, J.-H., Zhang, K., Zhang, H., and Zhou, C.: Radiative forcing of the direct aerosol effect from AeroCom Phase II simulations, Atmos. Chem. Phys., 13, 1853–1877, doi:10.5194/acp-13-1853-2013, 2013.

Nam, J., Wang, Y., Luo, C., and Chu, D. A.: Trans-Pacific transport of Asian dust and CO: accumulation of biomass burning CO in the subtropics and dipole structure of transport, Atmos. Chem. Phys., 10, 3297–3308, doi:10.5194/acp-10-3297-2010, 2010.

Park, R. J., Jacob, D. J., Chin, M., and Martin, R. V., Sources of carbonaceous aerosols over the United States and implications for natural visibility, J. Geophys. Res., 108, 4355, doi:10.1029/2002JD003190, 2003.

Park, R. J., Jacob, D. J., Field, B. D., Yantosca, R. M., and Chin, M., Natural and transboundary pollution influences on sulfate-nitrate-ammonium aerosols in the United States: implications for policy, J. Geophys. Res., 109, D15204, doi:10.1029/2003JD004473, 2004.

Patterson, E. M., Gillet, D. A., and Stockton, B. H.: Complex index of refraction between 300 and 700 nm for Saharan aerosol, J. Geophys. Res., 82, 3153–3160, doi:10.1029/JC082i021p03153, 1977.

Pratt, A. S. and Evans, J. L.: Potential impacts of the Saharan air layer on numerical model forecasts of North Atlantic tropical cyclogenesis, Weather Forecast., 24, 420–435, doi:10.1175/2008WAF2007090.1, 2009.

Prospero, J. M. and Carlson, T. N.: Vertical and areal distribution of Saharan dust over the western equatorial North Atlantic ocean, J. Geophys. Res., 77, 5255–5265, 1972.

Ramanathan, V., Ramana, M. V., Roberts, G., Kim, D., Corrigan, C., Chung, C., and Winker, D.: Warming trends in Asia amplified by brown cloud solar absorption, Nature, 448, 575–578, doi:10.1038/nature06019, 2007.

Ridley, D. A., Heald, C. L., and Ford, B.: North African dust export and deposition: A satellite and model perspective, J. Geophys. Res., 117, D02202, doi:10.1029/2011JD016794, 2012.

Russell, P. B., Hobbs, P. V., and Stowe, L. L.: Aerosol properties and radiative effects in the United States east coast haze plume: An overview of the Tropospheric Aerosol Radiative Forcing Observational Experiment (TARFOX), J. Geophys. Res., 104, 2213–2222, 1999.

Schepanski, K., Tegen, I., Todd, M. C., Heinold, B., Bönisch, G., Laurent, B., and Macke, A.: Meteorological processes forcing Saharan dust emission inferred from MSG-SEVIRI observations of subdaily dust source activation and numerical models, J. Geophys. Res., 114, D10201, doi:10.1029/2008JD010325, 2009.

Shell, K. M. and Somerville, R. C. J.: Direct radiative effect of mineral dust and volcanic aerosols in a simple aerosol climate model, J. Geophys. Res., 112, D03205, doi:10.1029/2006JD007197, 2007.

Sinyuk, A., Torres, O., and Dubovik O.: Combined use of satellite and surface observations to infer the imaginary part of refractive index of Saharan dust, Geophys. Res. Lett., 30, 1081, doi:10.1029/2002GL016189, 2003.

Sokolik, I. N. and Toon, O. B., Direct radiative forcing by anthropogenic mineral aerosols, Nature, 381, 681–683, 1996.

Su, L. and Toon, O. B.: Saharan and Asian dust: similarities and differences determined by CALIPSO, AERONET, and a coupled climate-aerosol microphysical model, Atmos. Chem. Phys., 11, 3263–3280, doi:10.5194/acp-11-3263-2011, 2011.

Tegen, I. and Fung, I., Contribution to the atmospheric mineral aerosol load from land surface modification, J. Geophys. Res., 100, 18707–18726, 1995.

Tegen, I. and Lacis A. A.: Modeling of particle size distribution and its influence on the radiative properties of mineral dust aerosol, J. Geophys. Res., 101, 19237–19244, doi:10.1029/95JD03610, 1996.

Tegen, I., Lacis, A. A., and Fung, I.: The influence on climate forcing of mineral aerosols from disturbed soils, Nature, 380, 419–422, 1996.

Tegen, I., Hollrig, P., Chin, M., Fung, I., Jacob, D., and Penner, J.: Contribution of different aerosol species to the global aerosol extinction optical thickness: Estimates from model results, J. Geophys. Res., 102, 23895–23915, 1997.

Uno, I., Harada, K., Satake, S., Hara, Y., and Wang, Z.: Meteorological Characteristics and dust distribution of the Tarim Basin simulated by the nesting RAMS/CFORS dust model, J. Meteorol. Soc. Jpn., 83A, 219–239, 2005.

VanCuren, R. and Cahill, T.: Asian aerosols in North America: Frequency and concentration of fine dust, J. Geophys. Res., 107, 4804, doi:10.1029/2002JD002204, 2002.

Wang, J., Xu, X., Henze, D. K., Zeng, J., Ji, Q., Tsay, S.-C., and Huang, J.: Top-down estimate of dust emissions through integration of MODIS and MISR aerosol retrievals with the GEOS-Chem adjoint model, Geophys. Res. Lett., 39, L08802, doi:10.1029/2012GL051136, 2012.

Wang, Y., Jacob, D. J., and Logan, J. A.: Global simulation of tropospheric O3-NO_x-hydrocarbon chemistry, 1. Model formulation, J. Geophys. Res., 103, 10713–10726, 1998.

Washington, R., Todd, M. C., Engelstaedter, S., Mbainayel, S., and Mitchell, F.: Dust and the low-level circulation over the Bodélé Depression, Chad: Observations from BoDEx 2005, J. Geophys. Res., 111, D03201, doi:10.1029/2005JD006502, 2006.

Weaver, C. J., Ginoux, P., Hsu, N. C., Chou, M.-D., and Joiner, J.: Radiative Forcing of Saharan Dust: GOCART model simulations Compared with ERBE data, J. Atmos. Sci., 59, 736–747, 2002.

Wesely, M. L.: Parameterization of surface resistance to gaseous dry deposition in regional-scale numerical models, Atmos. Environ., 23, 1293–1304, 1989.

Wielicki, B. A., Barkstrom, B. R., Harrison, E. F., Lee, R. B., Smith, G. L., and Cooper, J. E.: Clouds and the earth's radiant energy system (CERES): an earth observing system experiment, B. Am. Meteorol. Soc., 77, 853–868, 1996.

Won, J.-G., Yoon, S.-C., Kim, S.-W., Jefferson, A., Dutton, E. G., and Holben, B.: Estimation of direct radiative forcing of Asian dust aerosols with Sun/sky radiometer and lidar measurements at Gosan, Korea, J. Meteorol. Soc. Jpn., 82, 115–130, 2004.

Yoshioka, M., Mahowald, M. N., Conley, J. A., Collins, D. W., Fillmore, W. D., Zender, S. C., and Coleman, B. D.: Impact of Desert Dust Radiative Forcing on Sahel Precipitation: Relative Importance of Dust Compared to Sea Surface Temperature Variations, Vegetation Changes, and Greenhouse Gas Warming, J. Climate, 20, 1445–1467, 2007.

Young, S. A. and Vaughan, M. A.: The retrieval of profiles of particulate extinction from Cloud-Aerosol Lidar Infrared Pathfinder Satellite Observations (CALIPSO) data: Algorithm description, J. Atmos. Oceanic Technol., 26, 1105–1119, doi:10.1175/2008JTECHA1221.1, 2009.

Yu, H. B., Remer, L. A., Chin, M., Bian, H. S., Tan, Q., Yuan,T. L., and Zhang, Y.: Aerosols from Overseas Rival Domestic Emissions over North America, Science, 337, 566–569, 2012.

Zender, C. S., Bian, H., and Newman, D.: The mineral dust entrainment and deposition (DEAD) model: description and 1990s dust climatology, J. Geophys. Res, 108, 4416, doi:10.1029/2002JD002775, 2003.

Zhang, L., Kok, J., Henze, D. K., Li, Q. B., and Zhao, C.: Improving simulations of fine dust surface concentrations over the Western United States by optimizing the particle size distribution, Geophys. Res. Lett., 40, 3270–3275, doi:10.1002/grl.50591, 2013.

Zhao, L. and Zhao, S.: Diagnosis and simulation of a rapidly developing cyclone related to a severe dust storm in East Asia, Global Planet. Change, 52, 105–120, 2006.